Cycle-by-Cycle Average Input Current Sensing Method for LLC Resonant Topologies

Zhiyuan Hu, Yan-Fei Liu, and P. C. Sen

Department of Electrical and Computer Engineering
Queen's University
Kingston, Canada
zhiyuan.hu@queensu.ca, yanfei.liu@queensu.ca, senp@queensu.ca

Abstract—**Average input current is an important control parameter for many power supply control techniques, but it is difficult to obtain in LLC resonant topologies due to the irregular current waveform and the existence of circulation current. Conventional current sensing methods have low bandwidth and are inaccurate. This paper proposes a cycle-by-cycle average input current sensing method. It utilizes the series resonant capacitor to derive the average input current, thus is lossless, accurate, and low-cost. The proposed method can be extended to other topologies that include a series capacitor. Thus it is potentially advantageous in vast applications.**

I. INTRODUCTION

Average input current sensing is essential for current-mode control, load sharing, over current protection, and many other control techniques. However it has difficulties in LLC resonant topologies due to the following reasons.

1. The current waveform is not a regular shape and changes with different load conditions; therefore the average input current in each switching period cannot be conveniently derived from the peak current or any instantaneous current level. As a result, low-pass filtering is required in order to derive the average current signal, which limits the bandwidth that can be achieved by current-mode control.

2. In LLC resonant tank, there is a branch in parallel with the transformer or the load; therefore the sensed resonant current is the total current including the circulation current and the output current reflected to the primary side. As a result, the sensed current signal cannot accurately reflect the output current, which degrades the performance of load sharing and current-mode control.

Current transformer is a common method to sense current, as those enumerated in [1]. However they all rely on low-pass filtering to derive the average current signal.

Capacitive divider and the peak resonant capacitor voltage can be used to reflect the resonant current level, as described in [2]. However, they also require low-pass

filtering. Also, the diode rectifier introduces voltage drop which distorts the linearity of the output signal.

DCR method as described in [3] can be used to measure instantaneous inductor current, but cannot measure average current in resonant topologies.

Trajectory analysis reveals that, when a LLC converter is operating at the resonant frequency and during steady state, the resonant capacitor voltage at the high-side switch's turn-off point has a mathematical relation with the output current [4, 5]. However, the equations are only valid during steady state and when the switching frequency equals the resonant frequency, which is not always true.

This paper provides a cycle-by-cycle input current sensing method for LLC resonant topologies by sensing the voltage across the series resonant capacitor at a particular time instant; therefore it is lossless and low-cost. It accurately calculates the average input current and input power in each switching period; therefore it is very advantageous in current-mode control, load sharing, and other advanced digital control techniques that require real-time average current information. Half-bridge LLC resonant converter is used as an example in this paper; but the proposed method can apply to many other topologies that include a series capacitor, such as half-bridge and full-bridge, LLC and LCC, converters and inverters. It also can be extended to SEPIC and Ćuk converters especially when using nonlinear inductors. This paper is organized as follows: Section II describes the operation principle of proposed method; Section III discusses possible implementations in different applications; Section IV discusses sources of errors and a calibration method; Section V demonstrates simulation results; and Section VI demonstrates experimental results.

II. OPERATION PRINCIPLE

The input current from a voltage source to a resonant power stage often consists of forward current and reverse current due to the reactive resonant tank. The net input current can be represented by net input electric quantity in

each switching period. The net input electric quantity can be calculated from the voltage variation of the series resonant capacitor over the period that energy exchange takes place between the input voltage source and the resonant power stage. Because the net input electric quantity reflects input power, and the input power equals output power (assuming 100% efficiency), the net input electric quantity truthfully reflects the output power.

Refer to Fig. 1. For half-bridge topologies, the energy exchange period begins when the low-side switch is turned off, at which instant the resonant current begins to flow back to the input voltage source; the energy exchange period ends when the high-side switch is turned off, shortly after which the high-side junction capacitance is charged to the input voltage and the input current stops. Fig. 2 shows typical waveforms of half-bridge LLC converters. The energy exchange period can be identified

(a) The instant after low-side switch is turned off

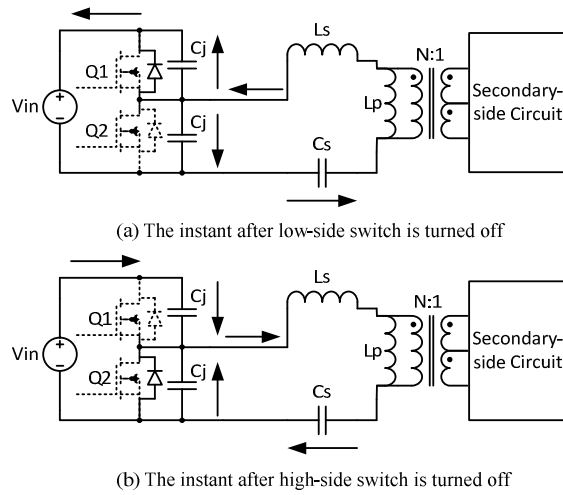(b) The instant after high-side switch is turned off

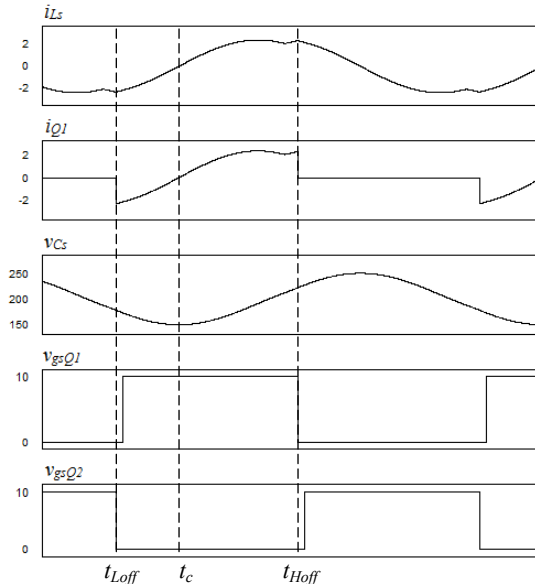Fig. 1. Initial and end instants of an energy exchange period.

Fig. 2. Typical waveforms of half-bridge LLC converter.

from the input current waveform i_{Q1}: there is negative input electric quantity from the low-side switch turn-off point t_{Loff} to the zero-crossing point t_c; and there is positive input electric quantity from t_c to the high-side switch turn-off point t_{Hoff}. The net input electric quantity can be calculated from the C_s voltage, v_{Cs}, at t_{Loff} instant and t_{Hoff} instant, as derived in (1).

$$Q_{net} = Q_{neg} + Q_{pos}$$
$$= C_s \left[v_{Cs}(t_c) - v_{Cs}(t_{Loff}) \right] + C_s \left[v_{Cs}(t_{Hoff}) - v_{Cs}(t_c) \right] \quad (1)$$
$$= C_s \left[v_{Cs}(t_{Hoff}) - v_{Cs}(t_{Loff}) \right]$$

A closer inspection of the energy exchange process reveals that the electric quantity resulted from the junction capacitances should be considered. Refer to Fig. 1. Shortly after t_{Loff}, the low-side junction capacitance is charged from 0V to V_{in} by the resonant current. In (1), this portion of electric quantity is considered as negative electric quantity back to the voltage source; in fact, it stays in the power stage; therefore it should be deducted from the negative input electric quantity. Similarly, shortly after t_{Hoff}, the input current continues to flow until the high-side junction capacitance is charged from 0V to V_{in}. This portion of electric quantity is not considered in (1); therefore, it should be added to the positive input electric quantity. As a result, the accurate net input electric quantity is derived in (2).

$$Q_{net} = C_s \left[v_{Cs}(t_{Hoff}) - v_{Cs}(t_{Loff}) \right] + 2C_j V_{in} \quad (2)$$

The net input current is derived in (3):

$$I_{in} = Q_{net} f_s$$
$$= C_s f_s \left[v_{Cs}(t_{Hoff}) - v_{Cs}(t_{Loff}) \right] + 2C_j f_s V_{in} \quad (3)$$

The net input power is derived in (4):

$$P_{in} = V_{in} I_{in}$$
$$= V_{in} C_s f_s \left[v_{Cs}(t_{Hoff}) - v_{Cs}(t_{Loff}) \right] + 2C_j f_s V_{in}^2 \quad (4)$$

Because the C_s voltage waveform is symmetrical to its DC component, for half-bridge topologies, there is:

$$\frac{V_{in}}{2} - v_{Cs}(t_{Loff}) = v_{Cs}(t_{Hoff}) - \frac{V_{in}}{2}$$
$$\Rightarrow v_{Cs}(t_{Hoff}) + v_{Cs}(t_{Loff}) = V_{in} \quad (5)$$

Thus (2), (3), and (4) can be simplified to (6), (7), and (8), respectively.

$$Q_{net} = C_s \left[2v_{Cs}(t_{Hoff}) - V_{in} \right] + 2C_j V_{in}$$
$$= C_s \left[V_{in} - 2v_{Cs}(t_{Loff}) \right] + 2C_j V_{in} \quad (6)$$

$$I_{in} = f_s C_s \left[2 v_{Cs}(t_{Hoff}) - V_{in} \right] + 2 C_j f_s V_{in}$$
$$= f_s C_s \left[V_{in} - 2 v_{Cs}(t_{Loff}) \right] + 2 C_j f_s V_{in} \quad (7)$$

$$P_{in} = V_{in} f_s C_s \left[2 v_{Cs}(t_{Hoff}) - V_{in} \right] + 2 C_j f_s V_{in}^2$$
$$= V_{in} f_s C_s \left[V_{in} - 2 v_{Cs}(t_{Loff}) \right] + 2 C_j f_s V_{in}^2 \quad (8)$$

Therefore, at steady state, by using (6), (7), or (8), the average input current and power can be monitored by sampling C_s voltage at only one point, either $v_{Cs}(t_{Hoff})$ or $v_{Cs}(t_{Loff})$. This is a simple and lossless method for applications that must exclude circulation current but don't need transient current information, such as load sharing.

When transient current information is needed, such as in current mode control, (2), (3), and (4) should be used to sense the average input current in each switching cycle, because the v_{Cs} waveform may not be symmetrical during transient.

A similar idea can be applied to full-bridge topologies, shown in Fig. 3. Let Q1 and Q2 be Leg A, and Q3 and Q4 be Leg B. The high-side switch of one leg and the low-side switch of the other leg are always turned on and off simultaneously, allowing energy transfers from the voltage source to the resonant tank in both half-switching periods. Therefore, the net electric quantity of both half-cycles should be counted in order to calculate the total input electric quantity. Because the two legs operate simultaneously, $v_{Cs}(t_{AHoff}) = v_{Cs}(t_{BLoff})$, and $v_{Cs}(t_{ALoff}) = v_{Cs}(t_{BHoff})$. Therefore there are only two sampling points. The equations are derived in (9)—(11).

$$Q_{net} = 2 C_s \left[v_{Cs}(t_{AHoff}) - v_{Cs}(t_{ALoff}) \right] + 4 C_j V_{in} \quad (9)$$

$$I_{in} = 2 C_s f_s \left[v_{Cs}(t_{AHoff}) - v_{Cs}(t_{ALoff}) \right] + 4 C_j f_s V_{in} \quad (10)$$

$$P_{in} = 2 V_{in} C_s f_s \left[v_{Cs}(t_{AHoff}) - v_{Cs}(t_{ALoff}) \right] + 4 C_j f_s V_{in}^2 \quad (11)$$

Note that when sampling $v_{Cs}(t_{ALoff})$, which is at the turn-off instant of Q2, C_s is tied to V_{in} through Q3. Therefore the voltage across C_s is V_{in} subtracting the
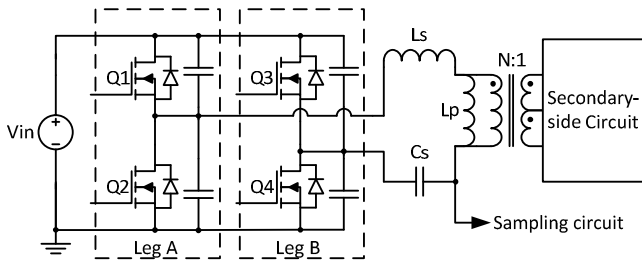

Fig. 3. Cycle-by-cycle current sensing in full-bridge topologies.

sampled voltage.

Further to (9)—(11), since $v_{Cs}(t_{AHoff}) = -v_{Cs}(t_{ALoff})$ in steady state, the equations can be further simplified, shown in (12)—(14).

$$Q_{net} = 4 C_s v_{Cs}(t_{AHoff}) + 4 C_j V_{in} \quad (12)$$

$$I_{in} = 4 C_s f_s v_{Cs}(t_{AHoff}) + 4 C_j f_s V_{in} \quad (13)$$

$$P_{in} = 4 V_{in} C_s f_s v_{Cs}(t_{AHoff}) + 4 C_j f_s V_{in}^2 \quad (14)$$

III. IMPLEMENTATIONS OF THE PROPOSED METHOD

Example implementations of the proposed cycle-by cycle average input current sensing method are shown in Fig. 4. The series resonant capacitor has one node connected to the ground, and the voltage of the other node is sampled by a controller. Digital controller with ADC peripheral is the most convenient solution, yet analog controller with a sample-and-hold circuit is also competent in some applications. The sampled signals are $v_{Cs}(t_{Hoff})$ and/or $v_{Cs}(t_{Loff})$, and then they are processed by an algorithm according to (1)—(8) to derive cycle-by-cycle average input current.

Depending on the applications, parameters such as input voltage, series capacitance, junction capacitance, and switching frequency may be omitted. Several variations of the proposed method are discussed as follows.

1) For load sharing application among interleaved identical resonant power stages, such as in topologies proposed in [6] and [7], input current in each phase should be calculated and balanced according to (7). But because the interleaved phases operate at the same switching frequency, the same input voltage, and use the same type of MOSFETs, f_s, V_{in}, and C_j are identical and thus can be eliminated from the equation. The C_s value
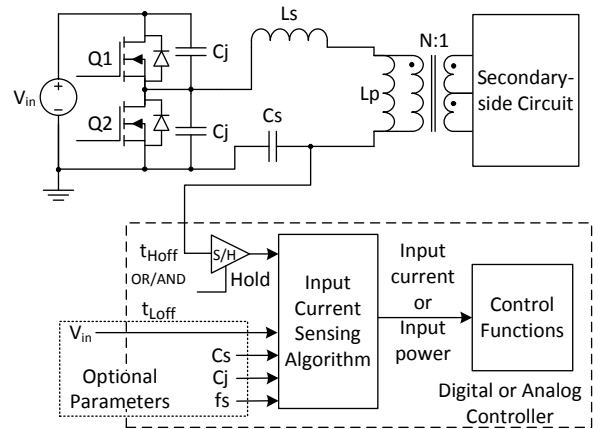

Fig. 4. Implementations of the proposed input current sensing method.

can be also eliminated from the equation since the component tolerance is small. Therefore, the load sharing loop's control objective is simply balancing the $v_{Cs}(t_{Hoff})$ or $v_{Cs}(t_{Loff})$ value in all the interleaved phases. No arithmetic is needed. In this case, the load sharing performance is only affected by the C_s tolerance. For example, if C_s has ±5% tolerance, the load sharing will have only ±5% error. As it will be shown further below in this paper, C_s in each power stage can be easily calibrated, and then the load sharing will be very accurate even with large component tolerances.

2) For current sharing among different energy sources, because the input voltage, switching frequency, and possibly the converter designs may be completely different, all the optional parameters in Fig. 4 should be used, and (8) should be used instead of (7). Above discussion is also true for power reporting applications.

3) In current mode control applications, (3) should be used. Because the feedback loop only requires a linear relation between the sensed signal and the actual output current level, the C_j term can be omitted because it does not affect the linearity of the measurement. The f_s parameter can be also omitted, because in small-signal scale the switching frequency changes very little. The C_s parameter can be omitted as well because it is a constant. As a result, the $[v_{Cs}(t_{Hoff}) - v_{Cs}(t_{Loff})]$ value is sufficient to reflect the net input current, and can be used for current mode control.

IV. Sources of Error and Calibration Method

Several sources may contribute to the error of the proposed current sensing method. They are usually small and do not affect the functionality of the intended applications such as load sharing and current mode control. For completeness they are discussed in this section. Also provided is a simple calibration method to compensate the errors.

A. Sources of Error

1) Value of C_j

The value of C_j includes output capacitance of the MOSFET, C_{oss}, and parasitic capacitance on the PCB. C_{oss} is a nonlinear capacitance that varies with the drain-to-source voltage of the MOSFET. A charge-equivalent linear capacitance must be derived from datasheet, which is the average value of the C_{oss}–V_{DS} curve from 0V to V_{in} [8]. Therefore, the equivalent C_j slightly differ at different input voltage. A simple calibration method is provided further below to determine the C_j value experimentally.

2) Value of C_s

As discussed in Section III, the resonant capacitor C_s has tolerance, which affects the measurement accuracy of the proposed method. Usually the resonant capacitor should have a small tolerance, e.g. ±5%; otherwise the power train's design margin has to be very large and thus compromises the performance. This is a favorable situation for the proposed method. In addition, a simple calibration method is provided further below to determine the C_s value experimentally.

3) Power loss

The proposed method measures input power from the primary side. If it is used to estimate the output power, power loss in the power stage will cause measurement error. Nevertheless, this inaccuracy exists in any primary-side current sensing method. A calibration method provided in the next section can compensate this error.

4) Propagation delay

MOSFET drivers usually have about 100 ns propagation delay. And depending on the strength of the driver, there is a delay from the driver output to the gate-to-source voltage falling below the gate threshold. Therefore, the sampling point should be delayed accordingly.

5) Sampling circuitry

The resonant capacitor voltage must be scaled down from several hundred volts to the ADC scale range; therefore a large resistor divider is required. However the maximum ADC input impedance is in the range of 100 Ω, therefore sampling errors may occur due to the high input impedance. An amplifier circuit is recommended to decouple the impedance.

B. Calibration Mehotd

A simple calibration method is provided to identify C_j and C_s values experimentally. The purpose of the calibration is not to get the accurate C_j and C_s values, but to match them with actual input power in order to get accurate measurement. The calibration has two steps:

1) Modulate the resonant power stage to a steady state at which $v_{Cs}(t_{Hoff}) = v_{Cs}(t_{Loff}) = V_{in}/2$ (half bridge). Then (3) can be reduced to (15):

$$I_{in} = 2C_j f_s V_{in} \qquad (15)$$

In (15), the input current and input voltage can be read from the input voltage source; the switching frequency can be directly measured; and then the equivalent C_j value can be solved.

2) Operate the resonant power stage at a medium load condition, measure $v_{Cs}(t_{Hoff})$ and $v_{Cs}(t_{Loff})$. Read input voltage and current from the input voltage source, and measure the switching frequency. With above information and the C_j value measured in Step (1), the equivalent C_s value can be solved using (3).

Above steps calibrate the C_j and C_s values with respect to input power. If the purpose is to measure the output power, calibrations should be performed with respect to the output power. In that case, the calibrated C_s value may be smaller than the actual value because the power loss is lumped into the calibrated C_s value. When the efficiency

changes, however, the measurement will have error. If this is a concern, multiple calibrations in different input/output conditions can be performed, and the measurement can use a corresponding set of calibration values in different operating conditions.

V. SIMULATION VERIFICATION

Simulation can provide accurate results and is free from component tolerance and measurement error, thus is the best approach to verify the theory of the proposed current sensing method. The simulation verification consists of two parts: (a) demonstrate the proposed method is accurate even in extreme operating conditions; (b) demonstrate the proposed method has better load sharing performance than conventional current sensing methods.

A. Accuracy Verification

In order to demonstrate the proposed method is accurate even in an extreme condition, e.g. ZVS is lost, MOSFET Rds(on) is relatively large, and switching frequency is very far from the resonant frequency, the following parameters are used in simulation.

Table I. Simulation parameters of an extreme operating condition.

Topology	Half-bridge LLC Converter
Input Voltage	400V
Output Voltage	12V
Transformer turns ratio	20:1
Parallel Inductance (Lp)	100 µH
Series Inductance (Ls)	4 µH
Series Capacitance (Cs)	100 nF
Junction Capacitance (Cj)	2 nF (each MOSFET)
Dead Time	200 ns
MOSFET Rds(on)	500 mΩ
Switching Frequency	100 kHz

The simulation waveforms are shown in Fig. 5, where VgQ1 and VgQ2 are gating signals of high-side and low-side MOSFETs, respectively; VCs is the voltage across the series capacitor; I(Ls) and I(Lp) are the current of the series and the parallel inductor, respectively; VHB is the half-bridge node voltage; and Iin is the input current.

The inductor current waveforms show that the switching frequency is very far from resonant frequency. The sharp edges of the half-bridge node voltage and the high pulses of the input current at the MOSFETs' turn-on points indicate that ZVS condition is lost. The measurement results are summarized in Table II. It demonstrates that the proposed method has only 0.566% error in such an extreme condition.

Table II. Comparison of calculation and simulation results.

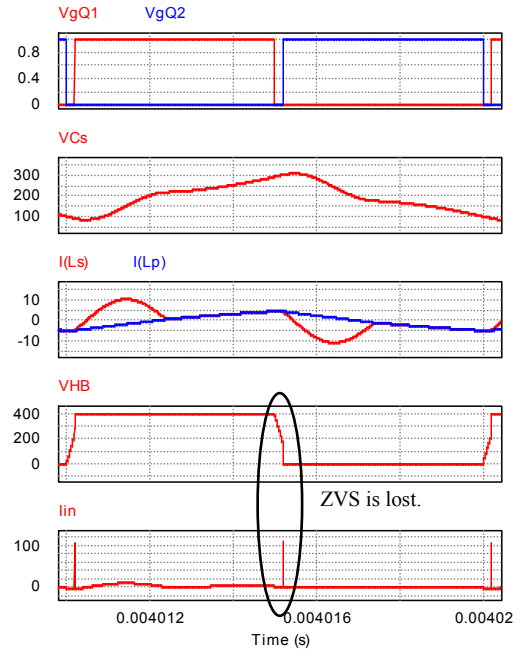| VCs (t$_{Loff}$)	105.925V
VCs (t$_{Hoff}$)	294.075V
Iin (calculated using the proposed method)	2.041A
Iin (measured from simulation waveform)	2.030A
Error	0.566%

Fig. 5. Simulation waveforms of a half-bridge LLC converter in an extreme operating condition.

B. Load Sharing Performance

In order to prove the proposed method has better load sharing performance than conventional current sensing methods, simulations of a two-phase interleaved LLC converter [6] are performed with different current sensing methods. The simulation parameters are shown in Table III.

Table III. Simulation parameters of an interleaved LLC converter.

Switching frequency	200kHz
Input Voltage	400V
Output Voltage	12V
Output Current	50A × 2
Transformer Turns Ratio	20:1
Parallel Inductance	99 µH (Phase1) 73 µH (Phase2)
Series Inductance	14 µH (Phase1) 10 µH (Phase2)
Series Capacitance	39 nF (Phase1) 33 nF (Phase2)
Junction Capacitance	2 nF (each MOSFET)
SCC Capacitance	30 nF
Output Capacitance	4 mF

The load sharing performance based on primary-side current transformer sensing method is shown in Fig. 6. It shows that although the resonant tank currents of the two phases are modulated to the same level, because their circulation currents differ, the output current are not balanced.

The load sharing performance based on peak resonant capacitor voltage sensing method is shown in Fig. 7. It is shown that although the peak resonant capacitor voltages of the two phases are modulated to the same level, the output currents are not well balanced.

171

The load sharing performance based on the proposed cycle-by-cycle current sensing method using to (6) is shown in Fig. 8. It demonstrates the most accurate load sharing performance among the three methods.
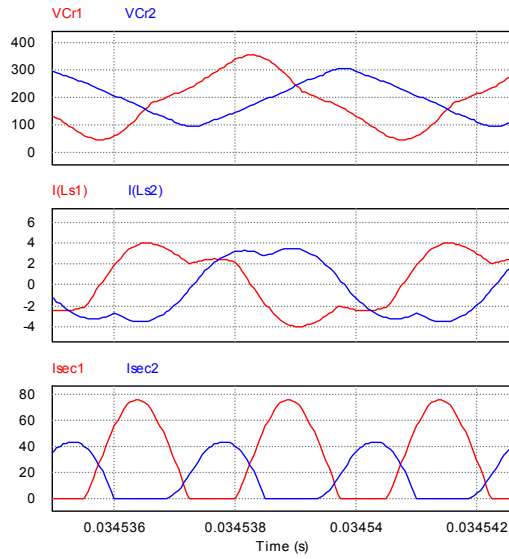

Fig. 6. Load sharing performance based on primary-side current transformer sensing method. Top: resonant capacitor voltage. Middle: resonant tank current. Bottom: output current.
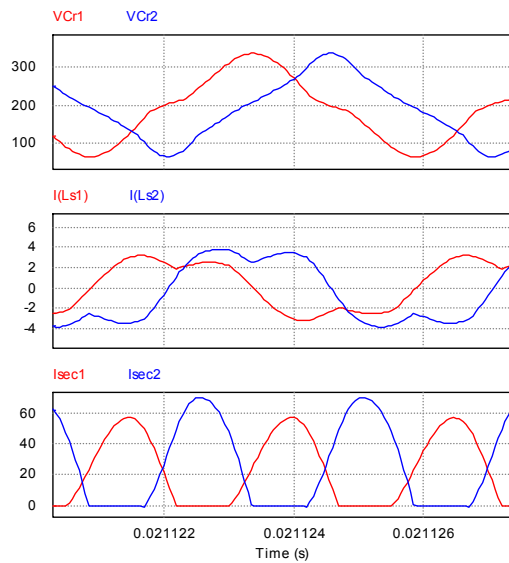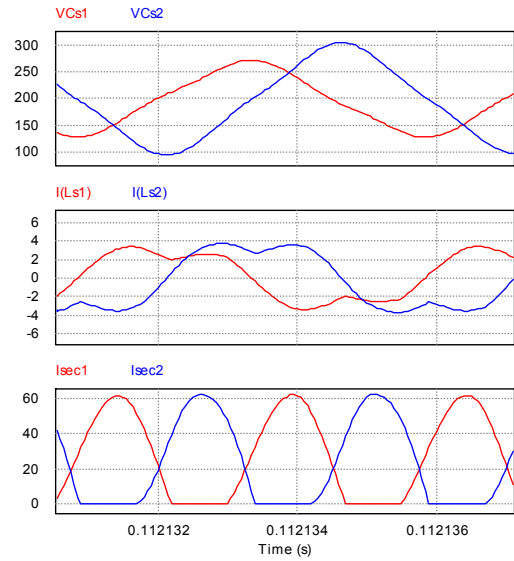

Fig. 7. Load sharing performance based on peak resonant capacitor voltage sensing method. Top: resonant capacitor voltage. Middle: resonant tank current. Bottom: output current.

Fig. 8. Load sharing performance based on the proposed cycle-by-cycle input current sensing method. Top: series resonant capacitor voltage. Middle: resonant tank current. Bottom: output current.

VI. EXPERIMENTAL VERIFICATION

The experimental verification consists of two parts: (a) waveform measurements on oscilloscope snapshots, proving that the proposed theory and calibration method are accurate; (b) demonstration of dynamic performances of a new control method that is derived from the proposed theory in this paper.

A. Accuracy Verification

A half-bridge LLC converter is used for experimental verification. The input voltage is 400V; the rated output is 12V/300W. C_s is calibrated to 36.8nF, and C_j is calibrated to 1.12nF by the calibration methods proposed in Section IV.B. Waveform snapshots of 5A, 10A, 15A, and 20A load conditions are shown in Fig. 9—Fig. 12. The cursor measurements shown on the screen read the C_s voltage at the high-side and low-side switches' turn-off points as well as the length of a half-switching period. The cursors are placed exactly at the 3V threshold voltage.

The experimental results are summarized in Table IV. Table IV demonstrates that the calculated input power values using the proposed method are highly consistent with the actual input power values. Note that in the case of Pin=71.6W, the Δv_{Cr} is 0, indicating all the input power is contributed by the second term of (4).

Table IV. Experimental data and calculation results based on cursor measurements.

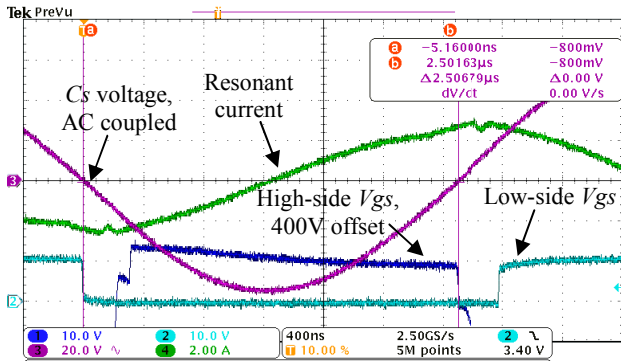| Load current	Actual P_{in} (read from source panel)	v_{Cs} at t_{Loff}	v_{Cs} at t_{Hoff}	f_s	Calculated P_{in}	Error
5A	**71.6 W**	199.2 V	199.2 V	199,458 Hz	**71.6 W**	0.00%
10A	**136.1 W**	188.8 V	211.2 V	197,348 Hz	**135.9 W**	-0.13%
15A	**199 W**	178.4 V	221.6 V	197,016 Hz	**196.0 W**	-1.50%
20A	**263.6 W**	166.4 V	233.6 V	195,483 Hz	**263.6 W**	-0.02%

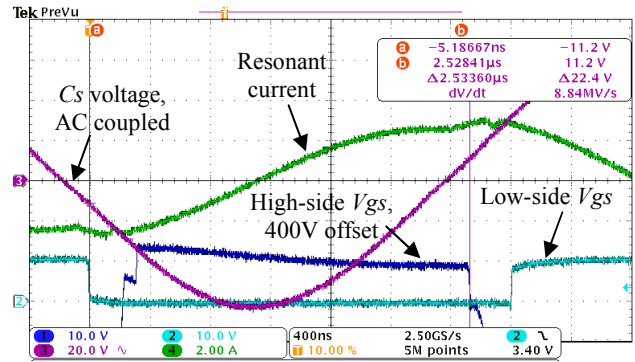Fig. 9. Waveform captured at 5A load.
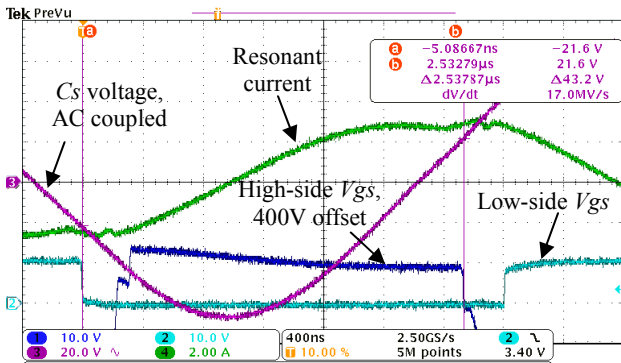

Fig. 10. Waveform captured at 10A load.
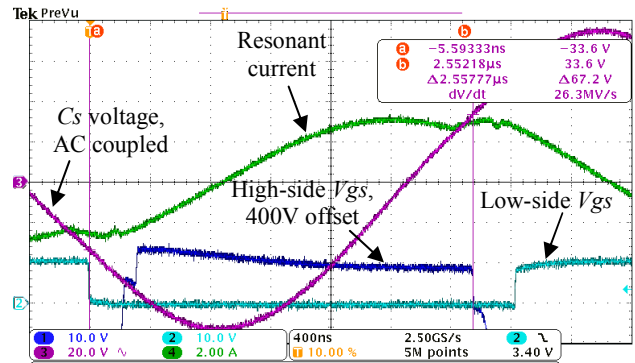

Fig. 11. Waveform captured at 15A load.

Fig. 12. Waveform captured at 20A load.

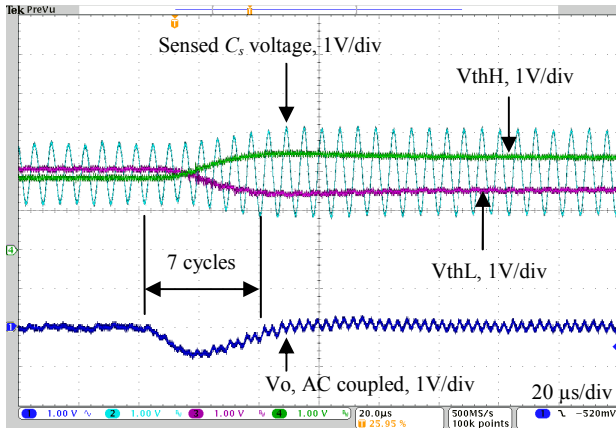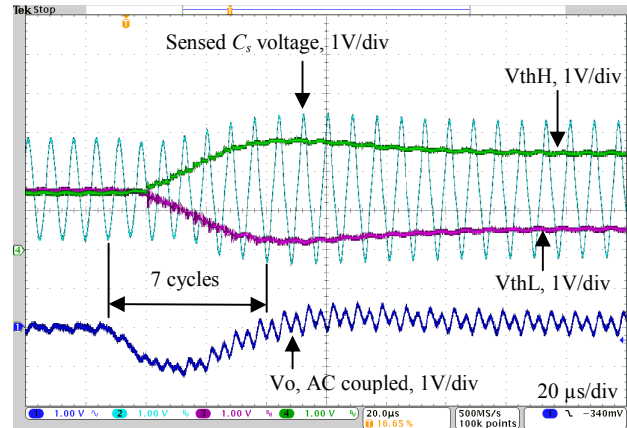Fig. 13. Load step from 5A to 25A (400V input).

Fig. 14. Load step from 5A to 25A (300V input).

B. Dynamic Control

A Bang-Bang Charge Control (BBCC) method is developed based on the proposed theory in this paper. This new control method is analogue to current-mode control, but it directly controls $v_{Cs}(t_{Hoff})$ and $v_{Cs}(t_{Loff})$ as thresholds to trigger the MOSFETs' switching, instead of using a voltage-controlled oscillator. As a result, the input electric quantity of each switching cycle is directly programmed without current sensing circuit. The loop bandwidth of a LLC converter using the BBCC method can achieve 1/6 of the switching frequency in all input voltage and load conditions with a simple PI or Type 2 controller.

Fig. 13 and Fig. 14 show 5A to 25A load step at 400V and 300V input voltage, respectively, where VthH is the internal threshold to trigger the high-side MOSFET to turn off, and VthL is the internal threshold to trigger the low-side MOSFET to turn off. In both waveforms, the output voltage is recovered within only 7 switching cycles responding to the load step. This is an outstanding performance for LLC converters.

More descriptions and analyses about the BBCC method are provided in [9].

173

VII. CONCLUSION

Average input current is an important control parameter for many power supply control techniques, but is difficult to obtain in LLC resonant topologies due to the irregular current waveform and the circulation current. Conventional current sensing methods are subject to error and slow response. This paper proposed a cycle-by-cycle average input current sensing method that is lossless, accurate, and low-cost. The operation principle, possible implementations, sources of error, and calibration method are discussed in this paper. The simulation and experimental results demonstrated good accuracy and the outstanding performances of the proposed method in load sharing and dynamic control. The proposed method can be extended to other topologies that include a series capacitor. Thus it is potentially advantageous in vast applications.

REFERENCES

[1] J. Jiang, Q. Wu, X. Xin, B. Wang, and H. Wu, "Current sensing signal comparing device, and current sensing signal comparing method," U. S. Patent 2011/0103112 A1, 2011.

[2] "L6599 high-voltage resonant controller," STMicroelectronics, , Datasheet, 2006.

[3] H. Lei and L. Shiguo, "Design considerations for small signal modeling of DC-DC converters using inductor DCR current sensing under time constants mismatch conditions," in *Proc. Power Electron. Specialists Conf. (PESC '07)*, 2007, pp. 2182-2188.

[4] W. Feng, F. C. Lee, and P. Mattavelli, "Optimal trajectory control of burst mode for LLC resonant converter," *IEEE Trans. Power Electron.,* vol. 28, pp. 457-466, 2013.

[5] W. Feng, F. C. Lee, and P. Mattavelli, "Simplified optimal trajectory control (SOTC) for LLC resonant converters," *IEEE Trans. Power Electron.,* vol. 28, pp. 2415-2426, 2013.

[6] Z. Hu, Y. Qiu, and Y.-F. Liu, "An interleaved LLC resonant converter operating at constant switching frequency," in *Proc. Energy Convers. Congr. and Expo. (ECCE'12)*, Raleigh, NC, 2012, pp. 3541-3548.

[7] Z. Hu, Y. Qiu, Y.-F. Liu, and P. C. Sen, "An interleaving and load sharing method for multiphase LLC converters," in *Proc. Appl. Power Electron. Conf. and Expo.(APEC '13)*, 2013, pp. 1421-1428.

[8] D. Costinett, R. Zane, and D. Maksimovic, "Circuit-oriented modeling of nonlinear device capacitances in switched mode power converters," in *Proc. Control Modeling Power Electron. (COMPEL'12)*, 2012, pp. 1-8.

[9] Z. Hu, L. Wang, Y.-F. Liu, and P. C. Sen, "Bang-bang charge control for LLC resonant converters," in *Proc. Energy Convers. Congr. and Expo. (ECCE'13)*, Denver, CO, 2013.